research paper

Acta Cryst C STRUCTURAL CHEMISTRY

ISSN 2053-2296

First COVID-19 molecular docking with a chalcone-based compound: synthesis, single-crystal structure and Hirshfeld surface analysis study

Mona A. Alsafi,[a] David L. Hughes[b]* and Musa A. Said[a]*

[a]Chemistry Department, College of Science, Taibah University, PO Box 30002, Al-Madinah Al Munawarah, Code 1417, Saudi Arabia, and [b]School of Chemistry, University of East Anglia, Norwich NR4 7TJ, England. *Correspondence e-mail: d.l.hughes@uea.ac.uk, masaid@taibahu.edu.sa

Received 29 June 2020
Accepted 25 October 2020

Edited by A. R. Kennedy, University of Strathclyde, United Kingdom

Keywords: chalcone; crystal structure; COVID-19; main protease; *in silico* molecular docking; Hirshfeld surface analysis (HSA).

CCDC reference: 2011624

Supporting information: this article has supporting information at journals.iucr.org/c

The first example of molecular docking of the SARS-CoV-2 main protease for COVID-19 [M^{pro}, Protein Data Bank (PDB) code 7BQY] by a chalcone-based ligand, namely, (*E*)-1-(2,4-dichlorophenyl)-3-[4-(morpholin-4-yl)phenyl]prop-2-en-1-one, $C_{19}H_{17}Cl_2NO_2$, **I**, is presented. Two-dimensional (2D) *LIGPLOT* representations calculated for the inhibitor **N3**, *viz*. *N*-{[(5-methylisoxazol-3-yl)-carbonyl]alanyl}-L-valyl-N_1-((1*R*,2*Z*)-4-(benzyloxy)-4-oxo-1-{[(3*R*)-2-oxopyrrolidin-3-yl]methyl}but-2-enyl)-L-leucinamide, and 7BQY are included for comparison with our chalcone-based complexes. The binding affinity of our chalcone ligand with 7BQY is −7.0 kcal mol^{-1}, a high value which was attributed to the presence of a hydrogen bond, together with many hydrophobic interactions between the drug and the active amino acid residues of the receptor. Docking studies were also performed, employing rigid and flexible binding modes for the ligand. The superposition of **N3** and the chalcone docked into the binding pocket of 7BQY is also presented. The synthesis, single-crystal structure, Hirshfeld surface analysis (HSA) and spectral characterization of heterocyclic chalcone-based compound **I**, are also presented. The molecules are stacked, with normal π–π interactions, in the crystal.

1. Introduction

COVID-19 is a worldwide disease that has currently infected over 47 million individuals with a death toll rate ranging from 5 to 9%. There are numerous ongoing efforts in drug discovery to control the awful impact of the disease on our lives (Jin *et al.*, 2020; Dhama *et al.*, 2020; Zhang & Liu, 2020; Peele *et al.*, 2020; Singhal, 2020). The SARS-CoV-2 main protease (M^{pro}) plays an important role in viral replication. In fact, it is a key target for COVID-19 drug discovery due to its low similarity with human genes. Other important roles in understanding the molecular mechanism in drug discovery are the binding affinity and structure of protein–drug complexes; hence, M^{pro} is well placed to serve as the primary drug target (Wang, 2020; Kumar *et al.*, 2020; Bhatia *et al.*, 2020). Chalcones containing heterocyclic substructures, *e.g.* 1,3-diphenyl-2-propen-1-one (Fig. 1), and many related compounds have attracted much interest because they show a range of pharmacological activities (Nowakowska, 2007; Kanagarajan & Gopalakrishnan, 2011; Thillainayagam *et al.*, 2016; Fu *et al.*, 2016; Burmaoglu *et al.*, 2020). Many reports have demonstrated that chalcone-based compounds have contributed in antimalarial (Larsen *et al.*, 2005), antitumour (Awoussong *et al.*, 2015), anti-inflammatory (Hsieh *et al.*, 1998), anti-oxidant (Nowakowska, 2007), antibacterial (Mallavadhani *et al.*, 2014) and antifungal (Wu *et al.*, 2014*a*) drugs. Also, well-established evidence shows that

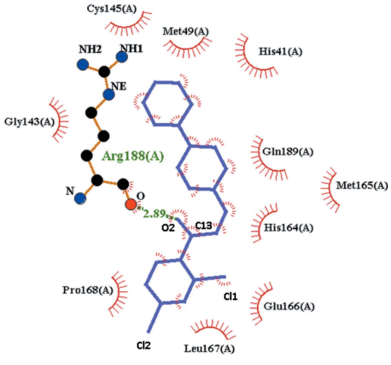

chalcone-based compounds can be inhibitors against the cysteine proteases in the malarial parasite which are responsible for the degradation of the host haemoglobin, known to be useful for the preparation of the amino acid, mainly cysteine (Cys) (Li *et al.*, 1995). Furthermore, they show an exciting healing feature, *viz.* relief of rheumatic pain (Nowakowska, 2007). Chalcones form a class of natural products present in tea, fruits, spices and vegetables. They are part of the flavonoid group comprising two aromatic rings joined by a three-carbon α,β-unsaturated carbonyl arrangement (Fig. 1) (Zi & Simoneau, 2005).

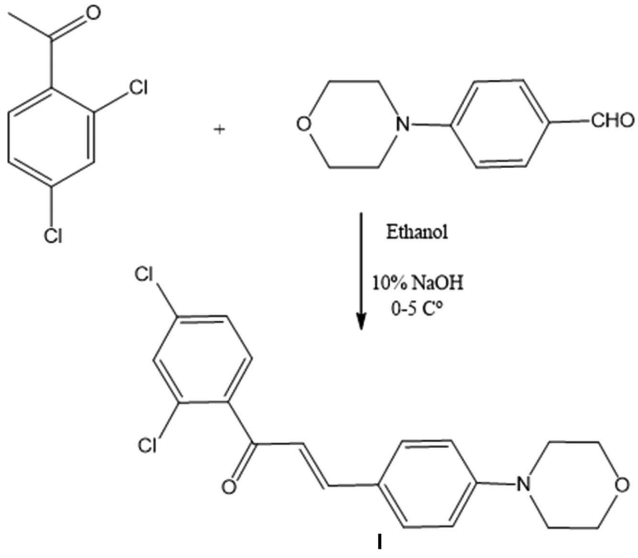

Scheme 1

We note, in this context, that chalcones can exist as *Z*- and/or *E*-isomers. Thermodynamic studies show that the *E*-isomer is the more stable (Larsen *et al.*, 2005). The *E*- and *Z*-isomers have been isolated and tested for their pharmacological action; only relatively small differences in the biological activities of the isolated isomers were observed (Larsen *et al.*, 2005).

At present, no effective clinical remedies are available for the treatment of COVID-19 (Ren *et al.*, 2020). Hence, the race for the characterization and identification of a new treatment candidate to inhibit binding between the COVID-19 main protease (M^{pro}) and the angiotensin converting enzyme-2, on the cell surface, is speeding up (Jin *et al.*, 2020). In view of these facts, we have been stimulated to screen, *in silico*, the interaction between the main protease (7BQY) active site with a heterocyclic chalcone-based ligand; we note that the first protein–ligand docking method was published more than three decades ago (Kuntz *et al.*, 1982).

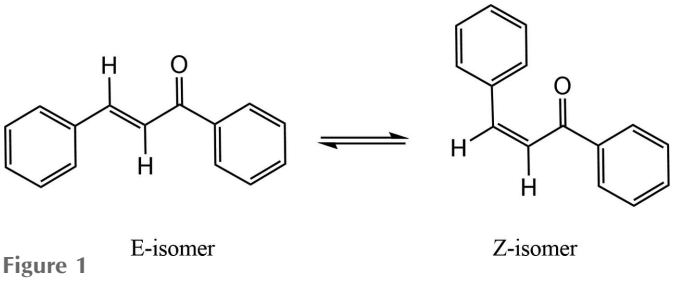

Figure 1
The *E* and *Z* isomers of the chalcone basic structure.

The X-ray structure of the COVID-19 main protease (M^{pro}) bonded to the inhibitor **N3**, *viz.* *N*-[(5-methylisoxazol-3-yl)-carbonyl]alanyl-L-valyl-N_1-((1*R*,2*Z*)-4-(benzyloxy)-4-oxo-1-{[(3*R*)-2-oxopyrrolidin-3-yl]methyl}but-2-enyl)-L-leucinamide, has been determined and refined, first to a resolution of 2.1 Å [Protein Data Bank (PDB) code 6LU7; Jin *et al.*, 2020] and later to a resolution of 1.7 Å (PDB code 7BQY; Liu *et al.*, 2020); the latter is therefore the preferred model for our studies. Schematic diagrams of protein–ligand interactions were generated using the *LIGPLOT* program (Wallace *et al.*, 1995); the plot for the inhibitor **N3** in its complex with 7BQY was used to identify the active sites and generate the receptor grid for docking simulations.

We also describe the synthesis of a heterocyclic chalcone-based compound (*E*)-1-(2,4-dichlorophenyl)-3-[4-(morpholin-4-yl)phenyl]prop-2-en-1-one or 2,4-$Cl_2C_6H_3$-CO-CH═CH-C_6H_4-*cyclo*-($NCH_2CH_2OCH_2CH_2$), **I** (Scheme 1), and report the single-crystal X-ray structure, Hirshfeld surface analysis (HSA) and spectral characterization, and from molecular docking studies, the likely binding of this molecule in the active site of 7BQY.

2. Experimental

2.1. General characterization techniques

All chemicals were purchased from Sigma–Aldrich and were used without further purification in the open atmosphere and at room temperature. Carbon, hydrogen and nitrogen contents were estimated on a CHN Model CE-440 Analyzer and on an Elementar Vario EL III Carlo Erbo 1108. IR spectra (ν/cm^{-1}) were recorded on an IRAffinity-1S Shimadzu instrument, using KBr disks. ^{1}H and ^{13}C NMR spectra were recorded with a Bruker AMX-400 spectrometer operating at 400 and 100 MHz using tetramethylsilane (TMS) as an internal standard.

2.2. Synthesis of chalcone I

To a stirred solution of 1-(2,4-dichlorophenyl)ethanone (0.188 g, 1 mmol) and 4-(morpholin-4-yl)benzaldehyde (0.191 g, 1 mmol) in ethanol (20 ml) at 0–5 °C was added dropwise 10% NaOH (10 ml). The resulting mixture was brought slowly to room temperature (25 °C) and then stirred for 12 h. The mixture was poured onto ice-cold water and acidified with HCl. The precipitate obtained was filtered off, washed with water (3 × 10 ml) and recrystallized from hot ethanol to produce the title compound as yellow crystals in good yield (74%; m.p. 139–142 °C) (Scheme 1). ^{1}H NMR ($CDCl_3$, 400 MHz): δ 3.43 (*s*, 4H, $NC\underline{H}_2CH_2O$), 3.65 (*s*, 4H, $NCH_2C\underline{H}_2O$), 6.03 and 6.07 (*d*, 2H, Ph), 7.50–8.03 (*m*, remaining Ph and C<u>H</u>═C<u>H</u>). IR (ν, cm^{-1}): 1512 and 1655 (C═C), 1575 (C═O), 1685 (C═O), 2857 and 2972 (C—H alkyl), 3089 (C—H aromatic). Analysis calculated (%) for $C_{19}H_{17}Cl_2NO_2$: C 63.00, H 4.73, N 3.87; found: C 63.32, H 4.91, N 4.05.

Table 1
Experimental details.

Crystal data	
Chemical formula	$C_{19}H_{17}Cl_2NO_2$
M_r	362.23
Crystal system, space group	Monoclinic, $P2_1$
Temperature (K)	100
a, b, c (Å)	3.96521 (9), 16.7005 (4), 12.4252 (2)
β (°)	91.185 (2)
V (Å^3)	822.63 (3)
Z	2
Radiation type	Cu $K\alpha$
μ (mm^{-1})	3.64
Crystal size (mm)	0.15 × 0.13 × 0.12
Data collection	
Diffractometer	Rigaku XtaLAB Synergy Dualflex HyPix
Absorption correction	Multi-scan (*CrysAlis PRO*; Rigaku OD, 2019)
T_{min}, T_{max}	0.790, 1.000
No. of measured, independent and observed [$I > 2\sigma(I)$] reflections	17673, 3089, 3079
R_{int}	0.028
(sin $\theta/\lambda)_{max}$ (Å^{-1})	0.618
Refinement	
$R[F^2 > 2\sigma(F^2)]$, $wR(F^2)$, S	0.024, 0.064, 1.07
No. of reflections	3089
No. of parameters	217
No. of restraints	1
H-atom treatment	H-atom parameters constrained
$\Delta\rho_{max}$, $\Delta\rho_{min}$ (e Å^{-3})	0.18, −0.20
Absolute structure	Flack x determined using 1385 quotients $[(I^+) - (I^-)]/[(I^+) + (I^-)]$ (Parsons *et al.*, 2013)
Absolute structure parameter	0.002 (9)

Computer programs: *CrysAlis PRO* (Rigaku OD, 2019), *SHELXT* (Sheldrick, 2015*a*), *ORTEP-3* (Farrugia, 2012), *SHELXL2018* (Sheldrick, 2015*b*) and *WinGX* (Farrugia, 2012).

2.3. Crystal structure analysis and refinement

H atoms were included in idealized positions and their U_{iso}(H) values were set to ride on the U_{eq} values of the parent C atoms. The absolute configuration is as shown in Fig. 2(*a*). In the final difference map, the highest peak (*ca* 0.2 e Å^{-3}) was near atom H18*a*. Experimental data for the crystals, the diffraction intensity measurements and the refinement procedure are given in Table 1.

2.4. Hirshfeld surface analysis

Hirshfeld surface analysis and the related two-dimensional (2D) fingerprint plots were calculated using *CrystalExplorer* (Version 17; Turner *et al.* 2017), which reads a structure input file in CIF format.

2.5. Docking *in silico* studies

Docking studies of chalcone ligand **I** were performed using the *Autodock Vina* wizard in *PyRx* 0.8 (available freely from https://sourceforge.net/projects/pyrx/). This is a powerful visualization engine, a more efficient and accurate tool than *AutoDock* 4, and a valuable software program for molecular docking (Allouche, 2012). The rigid and flexible binding modes of **I** were explored for comparison. The settings in the program include: Grid box (65, 65, 74 Å) centred at (6.057, −0.775, 22.695); energy range = 4 and exhaustiveness = 8; number of active torsion bonds set to zero in the case of the rigid ligand docking mode and four bonds for the flexible docking ligand mode. The same modes are possible for the protein using the default settings. *AutoDock Vina* offers two types of charges: 'Kollman' (used as the default setting) and 'Compute Gasteiger Charges' (calculated based on electronegativity equilibration; these can be applied on ligands where there are no partial charges, but may also be applied on the protein as well). Gasteiger charges assume an overall net neutral state for the molecular system, whereas Kollman charges define values for each amino acid derived from the corresponding electrostatic potential. The total Kollman charge added for the protein in this study was 4, with a value of zero for the ligand. The energy minimization of the protein was performed using the default settings in *Autodock Vina* in *PyRx*.

The chalcone molecular structure was taken from the X-ray analysis and the coordinates (in CIF format) were converted to PDB style for input to *Autodock Vina* in *PyRx*. The protease (PDB code 7BQY) was saved in PDB format after deletion of the water molecules and the **N3** ligand. The *PyMOL* molecular viewer was used to present the output and to measure the distances, angles and torsion angles among atoms of interest (DeLano, 2004). The key residues that form the substrate-binding pocket of 7BQY used in this study were identified from the binding mode of the protease with **N3** reported recently (Jin *et al.*, 2020) using the 2D *LIGPLOT* representation of the protein–ligand interactions in the complex (Wallace *et al.*, 1995); we note that these results confirm those reported in Fig. 2 of the *Extended Data* of the article by Jin *et al.*, (2020).

3. Results and discussion

3.1. Crystal structure analysis

A major feature of the chalcone-based structure of this study is that the keto–ethene group is shown to be the *E*-isomer. This can be seen clearly in the conformation (Fig. 2*a*) and the bond dimensions in the keto–ethene group (Ravishankar *et al.*, 2003).

Views of the chalcone molecule (with both the atom numbering and electron-density details) are shown in Fig. 2. X-ray analysis revealed that the molecule is a chain of three planar groups, *viz.* a phenyl ring, a keto–ethene group and a second phenyl group which is attached to a morpholine group (Fig. 2*a*). There is a rotation about the C1—C7 bond so that the normals to the planes of the C1–C6 phenyl ring and the linking keto–ethene group are 54.71 (12)° apart. The second phenyl ring, C11–C16, is rotated only 6.9 (2)° from the plane of the keto–ethene group, indicating that the keto–ethene fragment lies not far from the C11–C16 ring plane. The dihedral angle between the two phenyl ring planes is 50.21 (5)°, which is equal to the largest from earlier reported examples, *e.g.* 50.7° in 4-methylchalcone (Treadwell, 2006), 14.34° in 4-chlorochalcone (Li & Su, 1994) and 13.0° in chal-

Table 2
Torsion angles (°) of the keto–ethene group in selected chalcone molecules and of the keto–ethene group after ligand–protein interaction.

C16—C11—C9—C8	C11—C9—C8—C7	C9—C8—C7—O7	C9—C8—C7—C1	C8—C7—C1—C6	Reference
−7.4 (4)	−177.70 (19)	3.1 (4)	179.78 (19)	−128.2 (2)	This study
35.7	−177.6	20.2	−162.9	−47.3	This study*
11.0	−176.8	16.3	−163.0	−157.5	Treadwell (2006)
12.8	178.5	7.0	−173.0	169.0	Li & Su (1994)
2.5	−169.5	11.8	−179.8	163.8	Wu *et al.* (2014*b*)
−7.1	179.9	−8.5	170.7	166.8	Barsky *et al.* (2008); compound 3

Note: (*) the torsion angles for the keto–ethene after interaction with 7BQY.

Table 3
Bond lengths (Å) in the keto–ethene group in related chalcones (Ravishankar *et al.*, 2003).

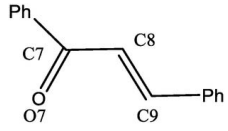

O7—C7	C7—C8	C8═C9	Reference
1.229 (3)	1.461 (3)	1.352 (3)	This study
1.224 (2)	1.474 (4)	1.326 (3)	Treadwell (2006)
1.227 (4)	1.474 (4)	1.313 (4)	Li & Su (1994)
1.240 (2)	1.459 (2)	1.327 (3)	Wu *et al.* (2014*b*)
1.226 (2)	1.471 (2)	1.325 (2)	Tang (2009)

cone itself (Wu *et al.*, 2014*b*). Our chalcone derivative has a torsion angle of 3.1 (4)° for the O7—C7—C8—C9 moiety; this is quite different from that in 4-methylchalcone (16.3°; Li & Su, 1994). There is almost a complete change of the torsion angles upon the calculated interaction of our chalcone with protease 7BQY (Table 2).

The three planar groups in our molecule are each stacked, with normal π–π interactions, along the *a* axis with interplanar distances of 3.65, 3.483 and 3.385 Å (Fig. 3). The C═C and C—C bonds in the bridging group are compared with other chalcone structures (Table 3); the C7—C8 single bond is generally slightly shorter than those reported, whereas C8═C9 is a longer double bond.

The C1–C6 arene ring is overlaid on one side by the corresponding ring in the molecule at (x + 1, y, z), with atom C5 over the ring centre, and on the other side by the ring in the molecule at (x − 1, y, z), with atom C2 over the ring centre. Similarly, the second ring has atom C15 of the molecule at (x + 1, y, z) over the C11–C16 ring centre and, on the other side, atom C12 of the molecule at (x − 1, y, z) is close to the ring centre. There are two further short intermolecular contacts, described as 'weak hydrogen bonds', *viz.* C18—H18*A*···O7^{i} and C13—H13···O7^{i} (see Table 4 for details).

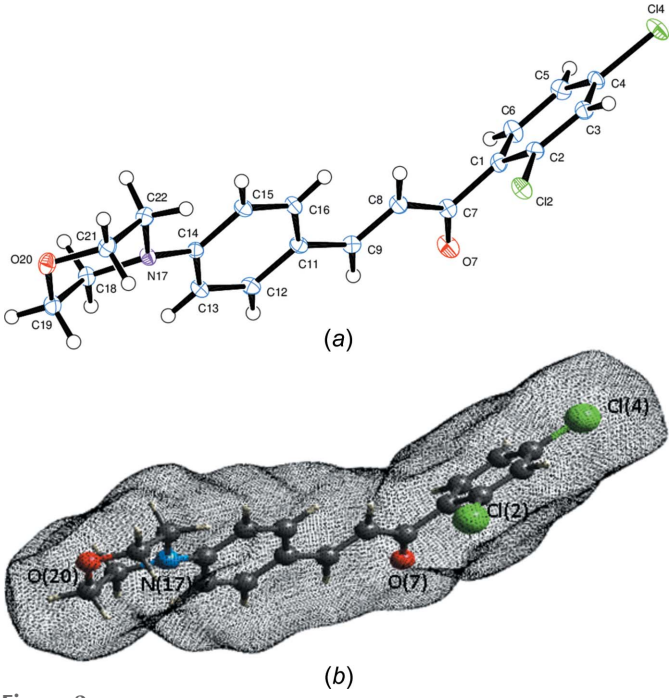

Figure 2
(*a*) View of a molecule of **I**, indicating the atom-numbering scheme. Displacement ellipsoids are drawn at the 50% probability level. (*b*) A mesh diagram of the compound showing the electron density around all the atoms of the molecule using the *CrystalExplorer* program with CIF data (Turner *et al.*, 2017).

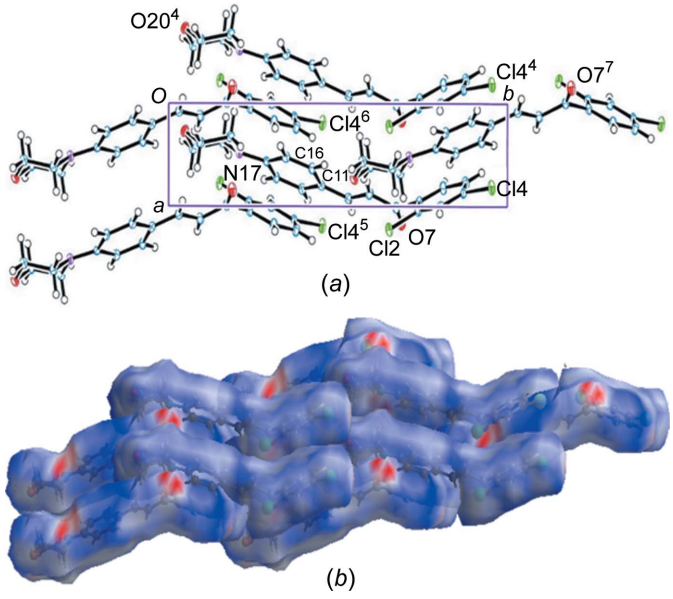

Figure 3
(*a*) The packing of molecules of **I**, viewed along the *c* axis. Molecules are stacked parallel to the *a* axis by overlap of each of the three planar groups. (*b*) The HSA d_{norm} map showing the molecular packing. Red indicates high-intensity contacts and blue indicates low-intensity contacts. [Symmetry codes: (4) $x-1, y, z$; (5) $-x+2, y-\frac{1}{2}, -z+1$; (6) $-x+1, y-\frac{1}{2}, -z+1$; (7) $-x+1, y+\frac{1}{2}, -z+1$.]

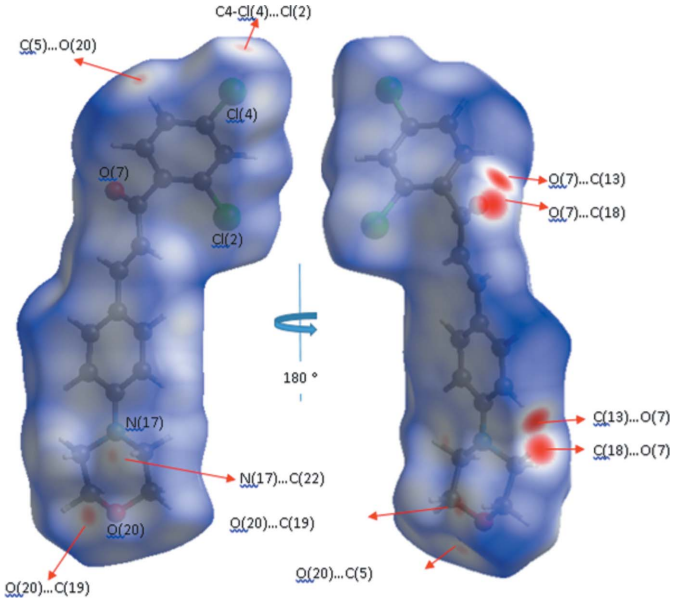

Figure 4
The HSA d_{norm} map of both sides of the molecule, showing C···O, C···N and C—Cl···Cl interactions observed between molecules. Blue indicates low-intensity contacts and red indicates high-intensity contacts.

3.2. Hirshfeld surface analysis

To help understand the supramolecular arrangement of our chalcone molecule, Hirshfeld surface analysis (HSA) was employed (Turner *et al.*, 2017). The d_e and d_i surfaces are illustrated in Fig. 4, where the red spots represent the points of closest interactions. The combination of d_i and d_e on a 'fingerprint' plot (Fig. 5) provides more information about all the contacts in the molecule. In fact, the intermolecular interactions (C—H···π, C—H···Cl, Cl4···Cl2, C—H···O and π–π) provide the stabilized molecular packing. These interactions connect the molecules in layers in the crystal packing. The Hirshfeld surface index map helps to analyse molecular contacts by colour code: blue indicates low-intensity contacts and red indicates high-intensity contacts (Aljohani *et al.*, 2019). The fingerprint plots show that H···H contacts constitute a high percentage of the interactions in the compound (37.8%). The C···H/H···C interactions act as secondary interactions with sharp peaks (14.4%). H···O/O···H contacts show slightly fewer interactions (12.6%) and the Cl···H/H···Cl contacts are unexpectedly high (20.6%), with total $d_i + d_e$ ($a + b$) $\simeq$ 2.85 Å, as can be seen in Fig. 5. Interestingly, π–π interactions account for 7.8%, indicating good π–π stacking. The region marked with a red dotted circle (light-blue region) represents the π–π interactions between rings; these are recognized by C···C contacts. The spikes due to the C—H···Cl and C···H contacts are pushed farther apart on the fingerprint plots, with $d_i + d_e \simeq$ 3.4 Å for each, corresponding to 20.6 and 14.4%, respectively, of all HS interactions.

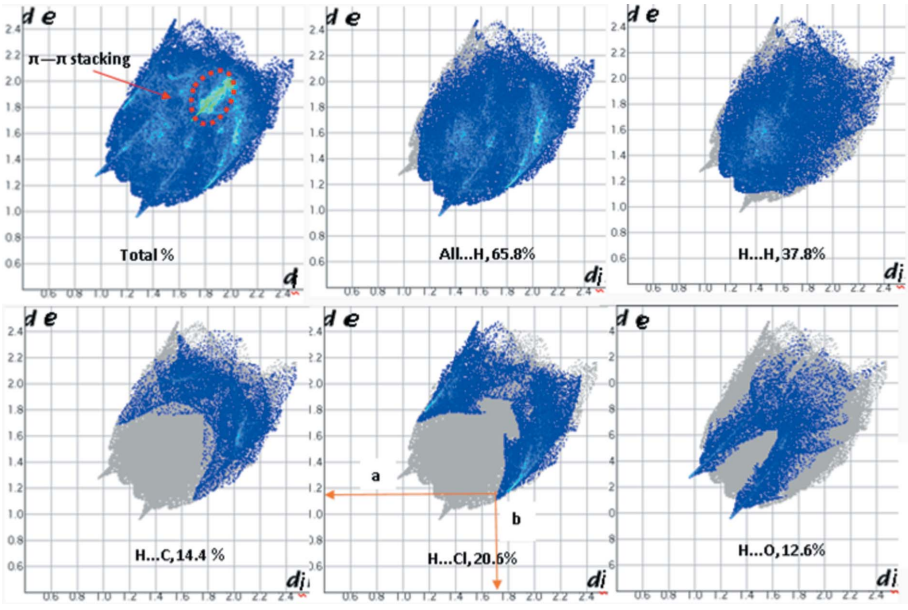

Figure 5
Hirshfeld surface fingerprint plots of the nearest internal distance (d_i) *versus* the nearest external distance (d_e) for chalcone **I**. d_i and d_e refer to intra- and intermolecular contacts, respectively.

Table 4
Hydrogen-bond geometry (Å, °).

D—H···A	D—H	H···A	D···A	D—H···A
C13—H13···O7^{i}	0.93	2.42	3.343 (3)	176
C18—H18A···O7^{i}	0.97	2.37	3.326 (3)	168

Symmetry code: (i) $-x+2, y-\frac{1}{2}, -z$.

3.3. Docking analysis

The purpose of this type of docking study, at this critical time, is to examine how a heterocyclic chalcone-based ligand might bind in the active site of the main protease for COVID-19 (M^{pro}; PDB code 7BQY). Predicting conformational changes of both the ligand and 7BQY is a challenge as both exhibit varying degrees of adjustment upon binding. Factors such as hydrogen bonding, hydrophobic interactions, solvation and entropy have direct effects on the structural reorganization. The docked molecule, fitted to interact with the active site of protease 7BQY, is shown in Fig. 6(*b*). The conformation of the chalcone molecule has been changed considerably from the conformation found in our single-crystal X-ray study, for a better fit in the site, as clearly manifested in the different values of the torsion angles (Table 2). It has been documented that the Gly143 amino acid residue in M^{pro} is the most attractive site for the formation of a hydrogen bond (Shah *et al.*, 2020); in our analysis, however, the contact is Arg188(A) (O)···O2—C13 of 2.89 Å

(Fig. 7*a*). Cys145, Glu166 and His163 are also strong amino acid residue candidates to form hydrogen bonds. The chalcone-based ligand interacts with 7BQY also through many hydrophobic interactions (Fig. 6*a*). A superposition diagram of the active sites of the 7BQY–**N3** compound with the docked 7BQY–chalcone compound was also drawn for best comparison of the docked chalcone compound in the active site of 7BQY (Fig. 6*b*). The residues of the active site of the protease 7BQY include: Arg188, Gln189, Met165, His164, Glu166, Cys145, Gly143, Leu167, Pro168, Met49 and His41. The cut-off for the nonbonded interactions (neglecting H atoms) between the ligand and the amino acid residues, for the *LIGPLOT* representations reported in this article, is 3.9 Å (Wallace *et al.*, 1995) (Fig. 6*a*).

Binding affinity is an important key to appreciate the strength of the binding interaction between the inhibitor (ligand or drug) and the biomolecule. It is affected by hydrogen bonding, electrostatic interactions and hydrophobic and van der Waals forces. The binding affinity obtained for our chalcone-based ligand with 7BQY is −7.0 kcal mol^{-1}. Recent docking studies on favipiravir, amodiaquine, 2′-fluoro-2′-deoxycytidine, ribavirin, hydroxychloroquine and remdesivir with 6LU7 showed binding affinities varying from −4.06 to −7.77 kcal mol^{-1}; hydroxychloroquine and remdesivir, with binding affinities of −6.06 and −4.96 kcal mol^{-1}, respectively, were approved drugs as inhibitors to SARS-CoV-2 M^{pro} (Hagar *et al.*, 2020). We note, now, however, that the FDA has recently revoked the approval for hydroxychloroquine (Thomson & Nachlis, 2020).

Table 5
Analysis results for all nine poses of the chalcone-based ligand with 7BQY.

Poses	Binding affinities (kcal mol^{-1})	RMSD lower limit	RMSD upper limit	No. of hydrogen bonds, residue, *D* (Å)
1	−7.0	0.0	0.0	1, Arg 188(A), 2.89
2	−7.0	1.535	2.045	3, Arg 188(A), 2.70; Gly 143(A), 3.08; Thr190(A), 3.10
3	−6.9	4.271	9.538	1, His164(A), 2.7
4	−6.8	1.291	1.722	1, Glu166(A), 2.68
5	−6.7	4.417	9.652	1, Gly143(A), 3.05
6	−6.7	5.001	10.53	1, Glu166(A), 3.00
7	−6.6	4.414	9.585	0
8	−6.6	2.759	3.767	1, Thr190(A), 2.70
9	−6.4	1.652	2.114	1, Glu166(A), 2.80

However, these and our results are far from the binding affinities found for disulfiram, trideglusib and shikonin drugs with 6LU7, *viz.* −46.16, −61.79 and −47.35 kcal mol^{-1}, respectively, reported by Jin *et al.* (2020).

Further docking studies were performed employing rigid and flexible binding modes for the chalcone-based ligand for a comparison of accuracy, time saving and entropy considerations (Alogheli *et al.*, 2017; Lorber & Shoichet, 1998). In rigid ligand docking mode to the protein binding site, the ligand is

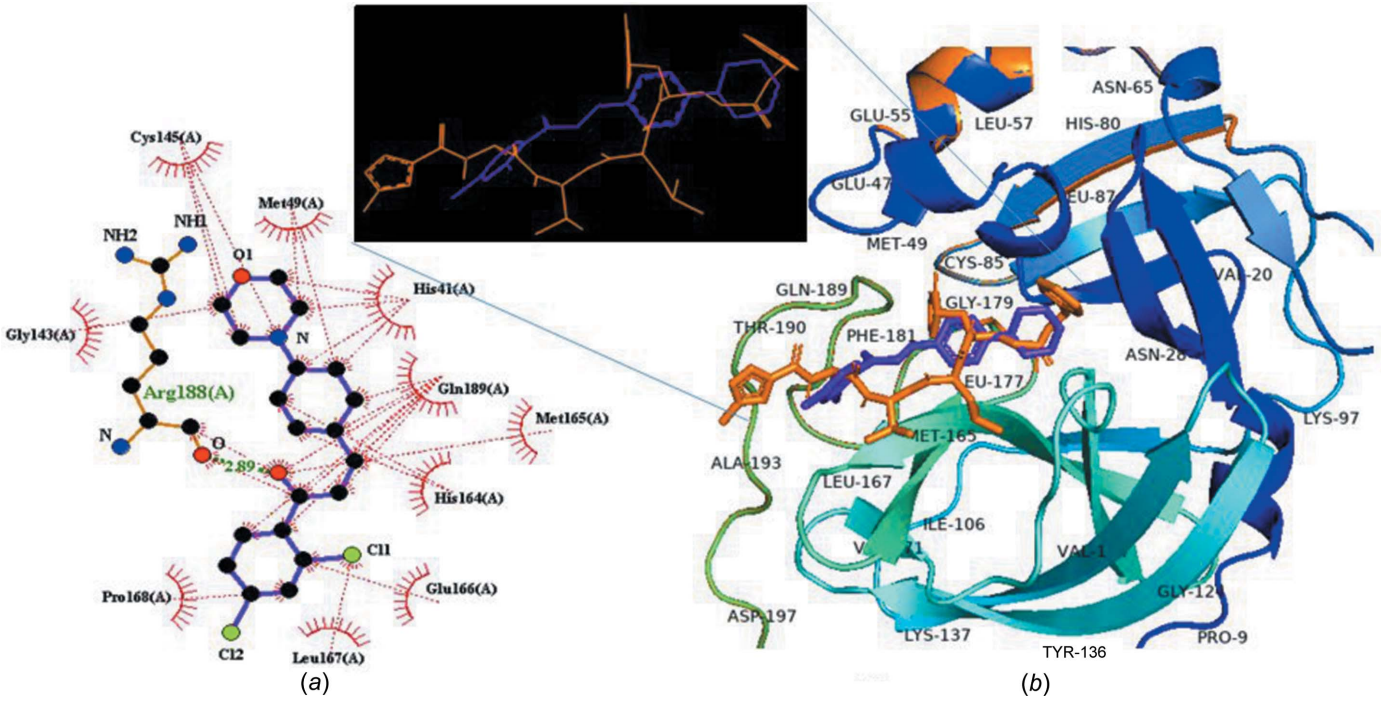

Figure 6
(*a*) A schematic 2D *LIGPLOT* representation of the SARS-CoV-2 main protease (M^{pro}; PDB code 7BQY) complex with chalcone **I**. The purple–blue stick, at the centre, represents the ligand, and the brown solid lines represent the active site (residue Arg188) involved in making a hydrogen bond with the ligand. The green dashed line represents the hydrogen bond and the thin red dashed lines and the spoked arcs pointing towards the ligand represent the hydrophobic residue bonds with the ligand. All atoms marked by spokes in the ligand or protein indicate atoms which are involved in the interactions. (*b*) The superposition of **N3** (orange stick) and chalcone **I** (purple–blue) docked into the binding pocket of 7BQY represented by *PyMOL* (DeLano, 2004). The small black window shows the two ligands in wire mode and the 7BQY residues have been omitted for clarity.

rotated relative to the binding site with no conformational changes of the ligand generated during the docking process. The binding affinities for the chalcone-based ligand with 7BQY, employing rigid ligand and flexible protein, flexible ligand and rigid protein, and flexible ligand and flexible protein are −7.0, −6.8 and −7.1 kcal mol^{-1}, respectively.

The binding affinity to the protein target is usually considered in selecting a possible drug candidate. Pose number 1 shows the highest binding affinity. The intermolecular interactions for the first three poses exhibit hydrogen bonding, whereas the rest suggest only hydrophobic interactions (Table 5).

In general, the molecular docking results show that the effective interactions of proteins with molecules involved the N and O atoms, and this could be attributed to the presence of lone-pair electrons on these atoms. Also, π–π stacking is a major contributor in hydrophobic interactions.

4. Conclusion

Crystal structure analysis of our chalcone compound shows it to be an *E*-isomer and to display significant deviations from planarity. In the keto–ethene group, the C—C bond is shorter and the C═C bond is longer than in other reported chalcones. The dihedral angle between the two benzene-ring planes is 60.21 **(?)**°, which is larger than in other chalcones and indicates a significant twist in the molecule. The intermolecular interactions (C—H···π, C—H···Cl, C—H···O and π–π) provide a stabilized molecular packing. These interactions connect the molecules to generate layers in the crystal packing.

Our chalcone derivative has been investigated as an inhibitor for COVID-19 by a molecular docking study. The binding affinity of the ligand in this study with 7BQY is −7.0 kcal mol^{-1}. Interestingly, the result revealed that the studied chalcone has a comparable binding affinity for SARS-CoV-2 main protease (PDB code 7BQY) to those of the approved medicines remdesivir and favipiravir, which have binding affinities of −6.96 and −4.06 kcal mol^{-1}, respectively, for SARS-CoV-2 main protease (PDB code 6LU7). This suggests that this chalcone may merit further study in the context of possible therapeutic agents for COVID-19. The binding affinity of the ligand with 7BQY was attributed to the presence of a hydrogen bond and many hydrophobic interactions between the drug and the active amino acid residues of the receptor.

Acknowledgements

MAS is grateful to AvH, Germany, for their continued support. MAS is also thankful to Dr Muniba Faiza, Editor of Bioinformatics Review, for many useful discussions.

References

Aljohani, G., Said, M. A., Lentz, D., Basar, N., Albar, A., Alraqa, S. Y. & Ali, A. A. (2019). *Molecules*, **24**, 1–14.
Allouche, A. (2012). *J. Comput. Chem.* **32**, 174–182.
Alogheli, H., Olanders, G., Schaal, W., Brandt, P. & Karlén, A. (2017). *J. Chem. Inf. Model.* **57**, 190–202.

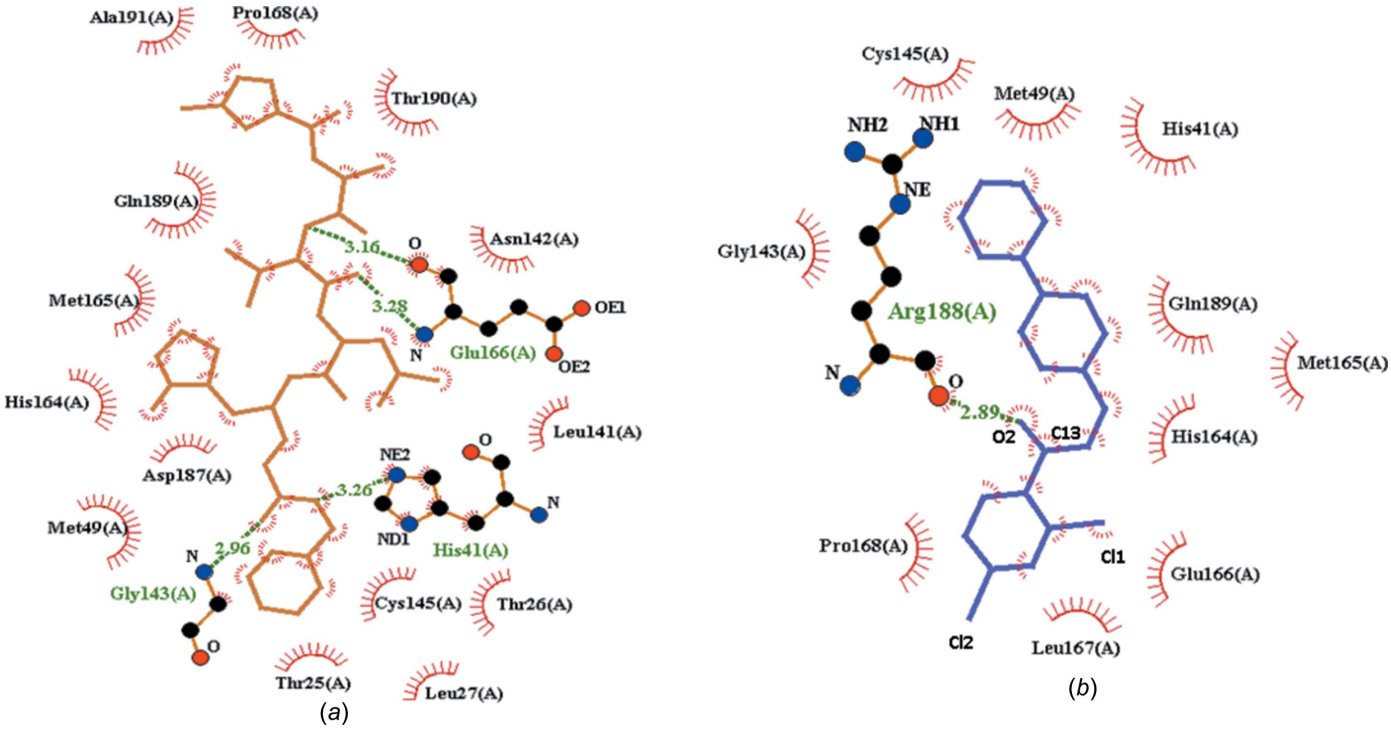

Figure 7
Schematic 2D *LIGPLOT* representations, calculated (*a*) for the inhibitor **N3** and the main protease (M^{pro}; PDB code 7BQY) and (*b*) for 7BQY with chalcone **I**, for comparison. A key to the symbols is given in Fig. 6. Only hydrogen bonds are shown and lines for hydrophobic interactions have been omitted for clarity.

Awoussong, P. K., Zaharia, V., Ngameni, B., Kuete, V., Ntede, H. N., Fokunang, C. N., Abegaz, B. M. & Ngadjui, B. T. (2015). *Med. Chem. Res.* **24**, 131–141.

Barsky, I., Bernstein, J., Stephens, P. W., Stone, K. H., Cheung, E., Hickey, M. B. & Henck, J. O. (2008). *Cryst. Growth Des.* **8**, 63–70.

Bhatia, S., Giri, S., Lal, A. F. & Singh, S. (2020). *Trop. Public Health*, **1**, 21–29.

Burmaoglu, S., Kazancioglu, E. A., Kaya, R., Kazancioglu, M., Karaman, M., Algul, O. & Gulcin, I. (2020). *J. Mol. Struct.* **1208**, 127868.

DeLano, W. L. (2004). *The pyMOL Molecular Graphics System*. DeLano Scientific LLC, San Carlos, CA, USA.

Dhama, K., Sharun, K., Tiwari, R., Dadar, M., Malik, Y. S., Singh, K. P. & Chaicumpa, W. (2020). *Hum. Vaccines Immunother.* **16**, 1232–1238.

Farrugia, L. J. (2012). *J. Appl. Cryst.* **45**, 849–854.

Fu, D. J., Zhang, S. Y., Song, J., Liu, Y. C., Zhang, L., Zhao, R. H., Zi, X. L., Liu, H. M. & Zhang, Y. B. (2016). *J. Chem. Res.* **40**, 620–623.

Hagar, M., Ahmed, H. A., Aljohani, G. & Alhaddad, O. A. (2020). *Int. J. Mol. Sci.* **21**, 3922–3935.

Hsieh, H. K., Lee, T. H., Wang, J. P., Wang, J. J. & Lin, C. N. (1998). *Pharm. Res.* **15**, 39–46.

Jin, Z., Du, X., Xu, Y., Deng, Y., Liu, M., Zhao, Y., Zhang, B., Li, X., Zhang, L., Peng, C., Duan, Y., Yu, J., Wang, L., Yang, K., Liu, F., Jiang, R., Yang, X., You, T., Liu, X., Yang, X., Bai, F., Liu, H., Liu, X., Guddat, L. W., Xu, W., Xiao, G., Qin, C., Shi, Z., Jiang, H., Rao, Z. & Yang, H. (2020). *Nature*, **582**, 289–293.

Kanagarajan, V. & Gopalakrishnan, M. (2011). *Pharm. Chem. J.* **45**, article No. 248.

Kumar, D., Chandel, V., Raj, S. & Rathi, B. (2020). *Chem. Biol. Lett.* **7**, 166–175.

Kuntz, I. D., Blaney, J. M., Oatley, S. J., Langridge, R. & Ferrin, T. E. (1982). *J. Mol. Biol.* **161**, 269–288.

Larsen, M., Kromann, H., Kharazmi, A. & Nielsen, S. F. (2005). *Bioorg. Med. Chem. Lett.* **15**, 4858–4861.

Li, R., Kenyon, G. L., Cohen, F. E., Chen, X., Gong, B., Dominguez, J. N., Davidson, E., Kurzban, G., Miller, R. E., Nuzum, E. O., Rosenthal, P. J. & McKerrow, J. H. (1995). *J. Med. Chem.* **38**, 5031–5037.

Li, Z. & Su, G. (1994). *Acta Cryst.* C**50**, 126–127.

Liu, X., Zhang, B., Jin, Z., Yang, H. & Rao, Z. (2020). RCSB Protein Data Bank (PDB) deposition code 7BQY.

Lorber, D. M. & Shoichet, B. K. (1998). *Protein Sci.* **7**, 938–950.

Mallavadhani, U. V., Sahoo, L., Kumar, K. P. & Murty, U. S. (2014). *Med. Chem. Res.* **23**, 2900–2908.

Nowakowska, Z. (2007). *Eur. J. Med. Chem.* **42**, 125–137.

Parsons, S., Flack, H. D. & Wagner, T. (2013). *Acta Cryst.* B**69**, 249–259.

Peele, K. A., Potla Durthi, C., Srihansa, T., Krupanidhi, S., Ayyagari, V. S., Babu, D. J., Indira, M., Reddy, A. R. & Venkateswarulu, T. C. (2020). *Informatics Med. Unlocked*, **19**, 100345.

Ravishankar, T., Chinnakali, K., Nanjundan, S., Selvamalar, C. S. J., Ramnathan, A., Usman, A. & Fun, H.-K. (2003). *Acta Cryst.* E**59**, o1143–o1145.

Ren, J. L., Zhang, A. H. & Wang, X. J. (2020). *Pharmacol. Res.* **155**, 104743.

Rigaku OD (2019). *CrysAlis PRO*. Rigaku Oxford Diffraction Ltd, Yarnton, Oxfrdshire, England.

Shah, B., Modi, P. & Sagar, S. R. (2020). *Life Sci.* **252**, 117652.

Sheldrick, G. M. (2015*a*). *Acta Cryst.* A**71**, 3–8.

Sheldrick, G. M. (2015*b*). *Acta Cryst.* C**71**, 3–8.

Singhal, T. (2020). *Indian J. Pediatr.* **87**, 281–286.

Tang, S. P., Kuang, D. Z., Feng, Y. L., Chen, M. S. & Li, W. (2009). *Acta Cryst.* E**65**, o1785.

Thillainayagam, M., Anbarasu, A. & Ramaiah, S. (2016). *J. Theor. Biol.* **403**, 110–128.

Thomson, K. & Nachlis, H. (2020). *JAMA*, **324**, 1282–1283.

Treadwell, E. M. (2006). *Acta Cryst.* E**62**, o5899–o5900.

Turner, M. J., Mckinnon, J. J., Wolff, S. K., Grimwood, D. J., Spackman, P. R., Jayatilaka, D. & Spackman, M. A. (2017). *CrystalExplorer*. Version 17. University of Western Australia.

Wallace, A. C., Laskowski, R. A. & Thornton, J. M. (1995). *Protein Eng. Des. Sel.* **8**, 127–134.

Wang, J. (2020). *J. Chem. Inf. Model.* **60**, 3277–3286.

Wu, J. Z., Cheng, C. C., Shen, L. L., Wang, Z. K., Wu, S. B., Li, W. L., Chen, S. H., Zhou, R. P. & Qiu, P. H. (2014*a*). *Int. J. Mol. Sci.* **15**, 18525–18539.

Wu, M.-H., Yang, X.-H., Zou, W.-D., Liu, W.-J. & Li, C. (2014*b*). *Z. Kristallogr. New Cryst. Struct.* **221**, 323–324.

Zhang, L. & Liu, Y. (2020). *J. Med. Virol.* **92**, 479–490.

Zi, X. & Simoneau, A. R. (2005). *Cancer Res.* **65**, 3479–3486.

supporting information

Acta Cryst. (2020). C**76**, 1043-1050 [https://doi.org/10.1107/S2053229620014217]

First COVID-19 molecular docking with a chalcone-based compound: synthesis, single-crystal structure and Hirshfeld surface analysis study

Mona A. Alsafi, David L. Hughes and Musa A. Said

Computing details

Data collection: *CrysAlis PRO* (Rigaku OD, 2019); cell refinement: *CrysAlis PRO* (Rigaku OD, 2019); data reduction: *CrysAlis PRO* (Rigaku OD, 2019); program(s) used to solve structure: SHELXT (Sheldrick, 2015a); program(s) used to refine structure: *SHELXL2018* (Sheldrick, 2015b); molecular graphics: *ORTEP-3* (Farrugia, 2012); software used to prepare material for publication: *SHELXL2018* (Sheldrick, 2015b) and *WinGX* (Farrugia, 2012).

(*E*)-1-(2,4-Dichlorophenyl)- 3-[4-(morpholin-4-yl)phenyl]prop-2-en-1-one

Crystal data

$C_{19}H_{17}Cl_2NO_2$
M_r = 362.23
Monoclinic, $P2_1$
a = 3.96521 (9) Å
b = 16.7005 (4) Å
c = 12.4252 (2) Å
β = 91.185 (2)°
V = 822.63 (3) Å^3
Z = 2
$F(000)$ = 376
D_x = 1.462 Mg m^{-3}
Cu $K\alpha$ radiation, λ = 1.54184 Å
Cell parameters from 17383 reflections
θ = 2.6–77.8°
μ = 3.64 mm^{-1}
T = 100 K
Prism, yellow
0.15 × 0.13 × 0.12 mm

Data collection

Rigaku XtaLAB Synergy Dualflex HyPix diffractometer
Radiation source: micro-focus sealed X-ray tube, PhotonJet (Cu) X-ray Source
Mirror monochromator
Detector resolution: 10.0000 pixels mm^{-1}
ω scans
Absorption correction: multi-scan (CrysAlis PRO; Rigaku OD, 2019)
T_{min} = 0.790, T_{max} = 1.000
17673 measured reflections
3089 independent reflections
3079 reflections with $I > 2\sigma(I)$
R_{int} = 0.028
θ_{max} = 72.4°, θ_{min} = 3.6°
h = −4→4
k = −17→20
l = −15→15

Refinement

Refinement on F^2
Least-squares matrix: full
$R[F^2 > 2\sigma(F^2)]$ = 0.024
$wR(F^2)$ = 0.064
S = 1.07
3089 reflections
217 parameters
1 restraint
Primary atom site location: dual
Hydrogen site location: inferred from neighbouring sites
H-atom parameters constrained
$w = 1/[\sigma^2(F_o^2) + (0.0463P)^2 + 0.1638P]$ where $P = (F_o^2 + 2F_c^2)/3$
$(\Delta/\sigma)_{max}$ < 0.001
$\Delta\rho_{max}$ = 0.18 e Å^{-3}
$\Delta\rho_{min}$ = −0.20 e Å^{-3}

Absolute structure: Flack *x* determined using 1385 quotients [(I+)-(I-)]/[(I+)+(I-)] (Parsons *et al.*, 2013)
Absolute structure parameter: 0.002 (9)

Special details

Geometry. All esds (except the esd in the dihedral angle between two l.s. planes) are estimated using the full covariance matrix. The cell esds are taken into account individually in the estimation of esds in distances, angles and torsion angles; correlations between esds in cell parameters are only used when they are defined by crystal symmetry. An approximate (isotropic) treatment of cell esds is used for estimating esds involving l.s. planes.

Refinement. The crystal used for analysis was a yellow cube cut down from a needle prism to *ca* 0.12 × 0.13 × 0.15 mm. This was mounted in oil on a small loop and fixed in the cold nitrogen stream on a Rigaku Oxford Diffraction XtaLAB Synergy diffractometer, equipped with Cu *Kα* radiation, HyPix detector and mirror monochromator. Intensity data were measured by thin-slice ω-scans. Total no. of reflections recorded, to θ_{max} = 72.5°, was 17673 of which 3089 were unique (R_{int} = 0.028); 3079 were 'observed′ with I > 2σ_I. Data were processed using the CrysAlisPro CCD and RED (Rigaku Oxford Diffraction Ltd., 2018) programs. The structure was determined by the intrinsic phasing routines in the SHELXT program (Sheldrick, 2015a) and refined by full-matrix least-squares methods, on F^2's, in SHELXL (Sheldrick, 2015b). The non-hydrogen atoms were refined with anisotropic thermal parameters.
Scattering factors for neutral atoms were taken from International Tables (1992). Computer programs used in this analysis have been noted above, and were run through WinGX (Farrugia, 2012) on a Dell Optiplex 780 PC at the University of East Anglia.
The crystallographic data were deposited at the Cambridge Crystallographic Data Centre (CCDC) under a CCDC number:2011624. Copies of the data can be obtained, via www. ccdc.cam.ac.uk.

Fractional atomic coordinates and isotropic or equivalent isotropic displacement parameters (Å²)

	x	*y*	*z*	U_{iso}*/U_{eq}
C1	0.9545 (5)	0.73931 (13)	0.27433 (17)	0.0152 (4)
C2	1.0426 (5)	0.73678 (13)	0.38359 (17)	0.0149 (4)
Cl2	1.22361 (12)	0.65138 (3)	0.44086 (4)	0.01875 (13)
C3	1.0024 (6)	0.80261 (15)	0.45034 (16)	0.0163 (4)
H3	1.067736	0.800400	0.522597	0.020*
C4	0.8631 (5)	0.87136 (14)	0.40690 (17)	0.0162 (4)
Cl4	0.81245 (14)	0.95350 (3)	0.49102 (4)	0.02188 (14)
C5	0.7663 (6)	0.87689 (14)	0.29907 (18)	0.0189 (4)
H5	0.670026	0.923528	0.271425	0.023*
C6	0.8174 (6)	0.81078 (14)	0.23391 (17)	0.0186 (4)
H6	0.758946	0.813997	0.161163	0.022*
C7	1.0117 (5)	0.67207 (13)	0.19629 (16)	0.0156 (4)
O7	1.1582 (4)	0.68791 (10)	0.11275 (13)	0.0218 (3)
C8	0.8765 (6)	0.59292 (15)	0.22078 (18)	0.0165 (4)
H8	0.758501	0.585203	0.283861	0.020*
C9	0.9208 (5)	0.53076 (14)	0.15283 (17)	0.0150 (4)
H9	1.047509	0.540990	0.092192	0.018*
C11	0.7933 (5)	0.45028 (14)	0.16393 (16)	0.0151 (4)
C12	0.8317 (5)	0.39453 (14)	0.08094 (17)	0.0160 (4)
H12	0.938062	0.410480	0.018466	0.019*
C13	0.7172 (5)	0.31664 (14)	0.08860 (17)	0.0155 (4)
H13	0.740596	0.281911	0.030725	0.019*
C14	0.5650 (5)	0.28933 (13)	0.18344 (16)	0.0132 (4)
C15	0.5209 (5)	0.34556 (14)	0.26673 (16)	0.0159 (4)

H15	0.415507	0.329814	0.329461	0.019*
C16	0.6316 (5)	0.42367 (14)	0.25670 (17)	0.0156 (4)
H16	0.598026	0.459444	0.312836	0.019*
N17	0.4798 (4)	0.20947 (12)	0.19637 (14)	0.0145 (4)
C18	0.3753 (5)	0.16042 (14)	0.10351 (16)	0.0165 (4)
H18A	0.500315	0.176468	0.040801	0.020*
H18B	0.137091	0.168634	0.087878	0.020*
C19	0.4400 (6)	0.07279 (14)	0.12729 (18)	0.0187 (4)
H19A	0.363274	0.040835	0.066366	0.022*
H19B	0.680642	0.064173	0.137077	0.022*
O20	0.2701 (4)	0.04708 (10)	0.22196 (13)	0.0193 (3)
C21	0.3857 (5)	0.09365 (14)	0.31143 (17)	0.0177 (4)
H21A	0.625238	0.084422	0.322896	0.021*
H21B	0.270985	0.076053	0.375454	0.021*
C22	0.3253 (5)	0.18248 (14)	0.29586 (17)	0.0161 (4)
H22A	0.084798	0.193057	0.292522	0.019*
H22B	0.421497	0.211782	0.356511	0.019*

Atomic displacement parameters (Å²)

	U^{11}	U^{22}	U^{33}	U^{12}	U^{13}	U^{23}
C1	0.0183 (10)	0.0116 (11)	0.0158 (10)	−0.0028 (8)	0.0015 (8)	0.0019 (8)
C2	0.0167 (10)	0.0114 (11)	0.0166 (10)	0.0002 (8)	0.0023 (8)	0.0020 (8)
Cl2	0.0279 (3)	0.0127 (3)	0.0157 (2)	0.00367 (18)	−0.00087 (17)	0.00193 (18)
C3	0.0182 (10)	0.0162 (11)	0.0144 (9)	−0.0017 (8)	0.0025 (7)	0.0003 (8)
C4	0.0198 (10)	0.0089 (10)	0.0201 (10)	−0.0020 (8)	0.0054 (8)	−0.0019 (8)
Cl4	0.0339 (3)	0.0124 (3)	0.0196 (2)	0.0030 (2)	0.00575 (19)	−0.00228 (19)
C5	0.0226 (11)	0.0131 (11)	0.0210 (11)	0.0018 (8)	0.0007 (8)	0.0033 (8)
C6	0.0267 (11)	0.0139 (11)	0.0151 (9)	0.0008 (8)	−0.0014 (8)	0.0018 (8)
C7	0.0190 (10)	0.0139 (12)	0.0139 (9)	0.0001 (8)	0.0000 (8)	0.0019 (8)
O7	0.0327 (8)	0.0164 (9)	0.0164 (7)	−0.0016 (6)	0.0067 (6)	0.0020 (6)
C8	0.0193 (10)	0.0149 (11)	0.0154 (10)	−0.0013 (8)	0.0027 (7)	0.0009 (8)
C9	0.0160 (10)	0.0155 (12)	0.0135 (9)	0.0009 (8)	0.0007 (7)	0.0023 (8)
C11	0.0160 (9)	0.0145 (11)	0.0148 (9)	0.0029 (8)	0.0003 (7)	0.0002 (8)
C12	0.0187 (10)	0.0150 (11)	0.0144 (9)	0.0014 (8)	0.0029 (8)	0.0012 (8)
C13	0.0190 (10)	0.0133 (11)	0.0143 (9)	0.0021 (8)	0.0011 (7)	−0.0010 (8)
C14	0.0130 (9)	0.0118 (11)	0.0146 (9)	0.0012 (7)	−0.0013 (7)	−0.0002 (8)
C15	0.0183 (10)	0.0167 (11)	0.0127 (9)	0.0008 (8)	0.0023 (7)	−0.0008 (8)
C16	0.0194 (10)	0.0134 (11)	0.0142 (9)	0.0001 (8)	0.0016 (8)	−0.0019 (8)
N17	0.0176 (8)	0.0120 (10)	0.0139 (8)	−0.0009 (7)	0.0014 (6)	−0.0008 (7)
C18	0.0186 (9)	0.0152 (12)	0.0156 (9)	−0.0017 (8)	−0.0004 (7)	−0.0004 (9)
C19	0.0191 (10)	0.0155 (12)	0.0214 (11)	−0.0017 (8)	−0.0003 (8)	−0.0016 (9)
O20	0.0201 (8)	0.0150 (9)	0.0227 (8)	−0.0043 (6)	−0.0010 (6)	0.0017 (6)
C21	0.0168 (10)	0.0158 (11)	0.0204 (10)	−0.0016 (8)	−0.0011 (8)	0.0031 (8)
C22	0.0170 (10)	0.0165 (12)	0.0148 (9)	−0.0018 (8)	0.0005 (7)	0.0019 (8)

Geometric parameters (Å, º)

C1—C2	1.396 (3)	C13—C14	1.411 (3)
C1—C6	1.400 (3)	C13—H13	0.9300
C1—C7	1.504 (3)	C14—N17	1.386 (3)
C2—C3	1.388 (3)	C14—C15	1.411 (3)
C2—Cl2	1.742 (2)	C15—C16	1.383 (3)
C3—C4	1.379 (3)	C15—H15	0.9300
C3—H3	0.9300	C16—H16	0.9300
C4—C5	1.389 (3)	N17—C22	1.462 (3)
C4—Cl4	1.739 (2)	N17—C18	1.468 (3)
C5—C6	1.387 (3)	C18—C19	1.514 (3)
C5—H5	0.9300	C18—H18A	0.9700
C6—H6	0.9300	C18—H18B	0.9700
C7—O7	1.229 (3)	C19—O20	1.433 (3)
C7—C8	1.461 (3)	C19—H19A	0.9700
C8—C9	1.352 (3)	C19—H19B	0.9700
C8—H8	0.9300	O20—C21	1.425 (3)
C9—C11	1.444 (3)	C21—C22	1.514 (3)
C9—H9	0.9300	C21—H21A	0.9700
C11—C12	1.400 (3)	C21—H21B	0.9700
C11—C16	1.403 (3)	C22—H22A	0.9700
C12—C13	1.382 (3)	C22—H22B	0.9700
C12—H12	0.9300		
C2—C1—C6	117.5 (2)	N17—C14—C15	121.41 (19)
C2—C1—C7	124.5 (2)	C13—C14—C15	117.3 (2)
C6—C1—C7	117.90 (18)	C16—C15—C14	121.16 (19)
C3—C2—C1	121.8 (2)	C16—C15—H15	119.4
C3—C2—Cl2	117.12 (16)	C14—C15—H15	119.4
C1—C2—Cl2	121.00 (17)	C15—C16—C11	121.6 (2)
C4—C3—C2	118.39 (19)	C15—C16—H16	119.2
C4—C3—H3	120.8	C11—C16—H16	119.2
C2—C3—H3	120.8	C14—N17—C22	120.14 (18)
C3—C4—C5	122.2 (2)	C14—N17—C18	120.77 (17)
C3—C4—Cl4	118.15 (17)	C22—N17—C18	112.09 (17)
C5—C4—Cl4	119.62 (18)	N17—C18—C19	110.01 (17)
C6—C5—C4	118.0 (2)	N17—C18—H18A	109.7
C6—C5—H5	121.0	C19—C18—H18A	109.7
C4—C5—H5	121.0	N17—C18—H18B	109.7
C5—C6—C1	122.0 (2)	C19—C18—H18B	109.7
C5—C6—H6	119.0	H18A—C18—H18B	108.2
C1—C6—H6	119.0	O20—C19—C18	111.65 (18)
O7—C7—C8	123.6 (2)	O20—C19—H19A	109.3
O7—C7—C1	117.66 (19)	C18—C19—H19A	109.3
C8—C7—C1	118.71 (18)	O20—C19—H19B	109.3
C9—C8—C7	120.8 (2)	C18—C19—H19B	109.3
C9—C8—H8	119.6	H19A—C19—H19B	108.0

C7—C8—H8	119.6	C21—O20—C19	109.14 (16)
C8—C9—C11	127.2 (2)	O20—C21—C22	112.81 (17)
C8—C9—H9	116.4	O20—C21—H21A	109.0
C11—C9—H9	116.4	C22—C21—H21A	109.0
C12—C11—C16	116.9 (2)	O20—C21—H21B	109.0
C12—C11—C9	120.35 (19)	C22—C21—H21B	109.0
C16—C11—C9	122.7 (2)	H21A—C21—H21B	107.8
C13—C12—C11	122.3 (2)	N17—C22—C21	110.01 (18)
C13—C12—H12	118.8	N17—C22—H22A	109.7
C11—C12—H12	118.8	C21—C22—H22A	109.7
C12—C13—C14	120.6 (2)	N17—C22—H22B	109.7
C12—C13—H13	119.7	C21—C22—H22B	109.7
C14—C13—H13	119.7	H22A—C22—H22B	108.2
N17—C14—C13	121.16 (19)		

C6—C1—C2—C3	−1.0 (3)	C16—C11—C12—C13	0.0 (3)
C7—C1—C2—C3	176.0 (2)	C9—C11—C12—C13	179.2 (2)
C6—C1—C2—Cl2	−178.56 (17)	C11—C12—C13—C14	−2.2 (3)
C7—C1—C2—Cl2	−1.6 (3)	C12—C13—C14—N17	−173.46 (19)
C1—C2—C3—C4	1.7 (3)	C12—C13—C14—C15	3.0 (3)
Cl2—C2—C3—C4	179.31 (17)	N17—C14—C15—C16	174.66 (19)
C2—C3—C4—C5	−0.7 (3)	C13—C14—C15—C16	−1.8 (3)
C2—C3—C4—Cl4	179.84 (16)	C14—C15—C16—C11	−0.3 (3)
C3—C4—C5—C6	−0.9 (3)	C12—C11—C16—C15	1.2 (3)
Cl4—C4—C5—C6	178.58 (17)	C9—C11—C16—C15	−178.0 (2)
C4—C5—C6—C1	1.5 (3)	C13—C14—N17—C22	179.40 (18)
C2—C1—C6—C5	−0.6 (3)	C15—C14—N17—C22	3.0 (3)
C7—C1—C6—C5	−177.8 (2)	C13—C14—N17—C18	−32.2 (3)
C2—C1—C7—O7	−128.3 (2)	C15—C14—N17—C18	151.44 (19)
C6—C1—C7—O7	48.7 (3)	C14—N17—C18—C19	155.90 (18)
C2—C1—C7—C8	54.8 (3)	C22—N17—C18—C19	−53.4 (2)
C6—C1—C7—C8	−128.2 (2)	N17—C18—C19—O20	57.1 (2)
O7—C7—C8—C9	3.1 (4)	C18—C19—O20—C21	−59.5 (2)
C1—C7—C8—C9	179.78 (19)	C19—O20—C21—C22	58.9 (2)
C7—C8—C9—C11	−177.70 (19)	C14—N17—C22—C21	−156.88 (18)
C8—C9—C11—C12	173.4 (2)	C18—N17—C22—C21	52.2 (2)
C8—C9—C11—C16	−7.4 (4)	O20—C21—C22—N17	−55.5 (2)

Hydrogen-bond geometry (Å, º)

D—H···*A*	*D*—H	H···*A*	*D*···*A*	*D*—H···*A*
C13—H13···O7^{i}	0.93	2.42	3.343 (3)	176
C18—H18*A*···O7^{i}	0.97	2.37	3.326 (3)	168

Symmetry code: (i) −*x*+2, *y*−1/2, −*z*.